Aerospace Science and Technology 52 (2016) 207–214

Contents lists available at ScienceDirect

Aerospace Science and Technology

www.elsevier.com/locate/aescte

XFOIL *vs* CFD performance predictions for high lift low Reynolds number airfoils

J. Morgado [a,*], R. Vizinho [b], M.A.R. Silvestre [a], J.C. Páscoa [b]

[a] University of Beira Interior, Aerospace Sciences Department, Edifício II das Engenharias, Calçada Fonte do Lameiro, no. 1, 6201-001 Covilhã, Portugal
[b] University of Beira Interior, Electromechanics Department, Edifício I das Engenharias, Calçada Fonte do Lameiro, no. 1, 6201-001 Covilhã, Portugal

ARTICLE INFO

Article history:
Received 16 December 2015
Received in revised form 24 February 2016
Accepted 26 February 2016
Available online 4 March 2016

Keywords:
XFOIL
Airfoil analysis
$k-kl-\omega$ modified transition model
$k-\omega$ SST turbulence model

ABSTRACT

Blade Element Momentum (BEM) theory is an extensively used technique for calculation of propeller aerodynamic performance. With this method, the airfoil data needs to be as accurate as possible. At the same time, Computational Fluid Dynamics (CFD) is becoming increasingly popular in the design and optimization of devices that depend on aerodynamics. For fixed and rotary wing applications, the airfoil lift over drag coefficient is the dominant airfoil performance parameter. Selecting a suitable computational tool is crucial for the successful design and optimization of this ratio. The XFOIL code, the Shear Stress Transport $k-\omega$ turbulence model and a refurbished version of $k-kl-\omega$ transition model were used to predict the airfoil aerodynamic performance at low Reynolds numbers (around 2.0×10^5). It has been shown that the XFOIL code gives the overall best prediction results. Also, it is not clear that CFD turbulence models, even with boundary layer transition detection capability, can compute better airfoil performance predictions data.

© 2016 Elsevier Masson SAS. All rights reserved.

1. Introduction

The technological developments in aeronautics, astronautics and material industries, together with the increase in oil prices caused by the world-wide oil crisis, brought a new focus on airship vehicles [1,2]. The Multibody Advanced Airship for Transportation (MAAT [3–6]) concept aims to develop a new global transportation form for people and goods. Generally, the propulsion system for these advanced low-dynamic vehicles is based on high power DC motor-driven propeller systems [1,7]. Nevertheless, at this altitude traditional propellers have a dramatically reduced efficiency caused by the high altitude atmosphere properties. When compared with lower altitude conditions, an airship operating in the stratosphere will find smaller air density and pressure as well as a reduced air kinematic viscosity and speed of sound. This makes the Reynolds number range of the propeller airfoils under study fall in the 10^5 order of magnitude and, simultaneously, limits the tip speed for a given limit Mach number. Thus, computational methods suitable for design and analysis of airfoils and propellers for high altitude operation are required. Blade Element Momentum theory (BEM) is commonly used to calculate the performance of propellers due to its low computational costs. However, the correct predictions from BEM codes depends on the reliability of the airfoil performance data [8]. Therefore, the correct estimation of the airfoil performance on the low Reynolds number regime found at high altitudes will have a decisive impact on the development of propellers for the MAAT airships. Airfoil performance at low Reynolds numbers is highly dependent on the boundary layer transition onset position [9]. So, it is essential to accurately predict the transition region on the surface of the airfoil to predict its actual performance. In order to analyze airfoils and make the coefficients available for use in the propeller performance prediction there are two main methods that can be applied. One is the solution of the Reynolds Averaged Navier Stokes (RANS) equations and closure models using structured or unstructured meshes. The second method is based on an inviscid flow solution coupled with a boundary-layer formulation. In order to study the accuracy of the above mentioned methods, a conventional $k-\omega$ SST turbulence model [10,11], a $k-kl-\omega$ transition closure [12] and XFOIL [13] were used to predict the performance of different airfoils at low Reynolds number.

The Shear Stress Transport $k-\omega$ model, is a two equation eddy-viscosity model developed by Menter et al. This SST formulation was devised to effectively blend the robust and accurate formulation of the $k-\omega$ model in the near wall region with the free-stream correct behavior of the $k-\varepsilon$ turbulence closure. The $k-kl-\omega$ transition model presents an interesting division of the turbulence scale introduced by Walters and Leylek [14]. The original model was implemented in OpenFoam and some modifications

* Corresponding author. Tel.: +351 96 748 06 76.
E-mail address: jmorgado@ubi.pt (J. Morgado).

http://dx.doi.org/10.1016/j.ast.2016.02.031
1270-9638/© 2016 Elsevier Masson SAS. All rights reserved.

Nomenclature

c	Airfoil local chord
C_D	Airfoil drag coefficient
C_L	Airfoil lift coefficient
D	Drag force, N
D'	Component of drag force on the original system of coordinates
D_L	$k-kl-\omega$ model laminar fluctuations kinetic energy destruction term
D_T	$k-kl-\omega$ model turbulent kinetic energy destruction term
D_ω	Cross diffusion term
f_ω	$k-kl-\omega$ model kinematic wall effect damping function
G_ω	Generation of ω
$\tilde{G}_k$	Turbulence kinetic energy generation due to mean velocity gradients
k	Turbulent kinetic energy
L	Lift force, N
L'	Component of lift force on the original system of coordinates
P_{kl}	$k-kl-\omega$ model laminar fluctuations kinetic energy production term
$P_{k_{t,s}}$	$k-kl-\omega$ model turbulent kinetic energy production term
R_{BP}	$k-kl-\omega$ model bypass transition energy transfer function
R_{NAT}	$k-kl-\omega$ model natural transition energy transfer function
S_k, S_ω	Dissipation of k and ω
t	Airfoil thickness
α	Angle of attack
ρ	Air density, kg/m^3
Γ_k, Γ_ω	Effective diffusivity of k and ω
μ	Dynamic viscosity, Pa s

were proposed [12]. The other used code was XFOIL. The XFOIL code [13] combines a panel method and an integral boundary layer formulation for the analysis of potential flow around the airfoils. The code was developed to rapidly predict the airfoil performance at low Reynolds numbers and its accuracy is well recognized [15].

2. Theoretical formulation

2.1. Shear stress transport (SST) $k-\omega$ model

As previously mentioned, the Shear Stress Transport (SST) $k-\omega$ model [10,11] is a two-equation eddy-viscosity closure. This Menter's *SST* formulation was developed to effectively blend the robust and accurate formulation of the standard $k-\omega$ turbulence model in the near wall region with the $k-\varepsilon$ model behavior as the model switches to the latter away from the wall. The authors decided to choose the SST $k-\omega$ model due to its accuracy for a wide class of low Reynolds number airfoil flows on which low Reynolds number airfoils are inserted, as suggested in the literature [16]. The SST $k-\omega$ model has similar formulation to the Standard $k-\omega$ model. The transport equations are defined as presented in Eq. (1) and Eq. (2):

$$\frac{\partial}{\partial t}(\rho k)+\frac{\partial}{\partial x_i}(\rho k u_i)=\frac{\partial}{\partial x_j}\left(\Gamma_k\frac{\partial k}{\partial x_j}\right)+\tilde{G}_k-Y_k+S_k \tag{1}$$

$$\frac{\partial}{\partial t}(\rho\omega)+\frac{\partial}{\partial x_i}(\rho\omega u_i)=\frac{\partial}{\partial x_j}\left(\Gamma_\omega\frac{\partial \omega}{\partial x_j}\right)+G_\omega-Y_\omega+D_\omega+S_\omega \tag{2}$$

The $\tilde{G}_k$ represents the generation of turbulence kinetic energy due to the mean velocity gradients, calculated according Eq. (3):

$$G_k=-\rho\overline{u_i'u_j'}\frac{\partial u_j}{\partial x_i} \tag{3}$$

The effective diffusivities for the $k-\omega$ model are given by Eq. (4) and Eq. (5):

$$\Gamma_k=\mu+\frac{\mu_t}{\sigma_k} \tag{4}$$

$$\Gamma_\omega=\mu+\frac{\mu_t}{\sigma_\omega} \tag{5}$$

where σ_k and σ_ω are the turbulent Prandtl numbers for k and ω respectively and they are calculated as presented in Eq. (6) and Eq. (7):

$$\sigma_k=\frac{1}{\frac{F_1}{\sigma_{k,1}}+\frac{(1-F_1)}{\sigma_{k,2}}} \tag{6}$$

$$\sigma_\omega=\frac{1}{\frac{F_1}{\sigma_{\omega,1}}+\frac{(1-F_1)}{\sigma_{\omega,2}}} \tag{7}$$

The turbulent viscosity μ_t (see Eq. (4) and Eq. (5)) is computed as follows:

$$\mu_t=\frac{\rho k}{\omega}\frac{1}{\max[\frac{1}{\alpha^*},\frac{SF_2}{a_1\omega}]} \tag{8}$$

where S represents the strain rate magnitude.

2.1.1. Low Reynolds correction

The low Reynolds correction implemented in Ansys Fluent® modifies the α^* coefficient (see Eq. (8)). This coefficient damps the turbulent viscosity and it is given by Eq. (9):

$$\alpha^*=\alpha^*_\infty\left(\frac{\alpha^*_0+Re_t/R_k}{1+Re_t/R_k}\right) \tag{9}$$

where:

$$Re_t=\frac{\rho k}{\mu\omega} \tag{10}$$

$$R_k=6 \tag{11}$$

$$\alpha^*_0=\frac{\beta_i}{3} \tag{12}$$

$$\beta_i=0.072 \tag{13}$$

Note that in the high-Reynolds-number form of the $k-\omega$ model, $\alpha^*=\alpha^*_\infty=1$.

2.2. $k-kl-\omega$ transition model

The work of Mayle and Schulz [17], was responsible for setting the foundations for the laminar kinetic energy theory. The latter theory accounts for the kinetic energy of the velocity fluctuations that occur within the laminar boundary layer pre-transitional region. These velocity oscillations were measured for the first time in 1937 as a result of the pioneer experimental work of Dryden

[18]. It was concluded that the free-stream turbulence was responsible for the occurrence of such boundary layer perturbations. Taylor [19] made an interesting observation regarding these pre-transitional laminar velocity fluctuations. It was acknowledged that these oscillations were related to thickening and thinning of the boundary layer. Later in 1971, the experimental work of Klebanoff [20], explicitly identified these streamwise fluctuations, naming them as breathing modes. However, through the work of Kendall [21] these velocity oscillations were renamed as Klebanoff modes in honor of their original discoverer.

Based on this new transition theory, many novel RANS transition models have been developed since then. In 2004, the numerical work of Walters and Leylek [14] presented a locally formulated laminar fluctuation kinetic energy transition model. The turbulence transition closure was named $k-kl-\omega$, and was implemented in the commercial software Ansys Fluent®. Later in 2008, Walters and Cokljat [22] presented an improved version of the original 2004 transition model, the $k-kl-\omega$. Besides the change in the turbulence length scale variable from ϵ to ω some model constants and functions were also modified. The $k-kl-\omega$ transition model can be resumed down to three transport equations. One for the laminar fluctuations kinetic energy, kl, another for the turbulent kinetic energy, k, and the last one for the specific turbulent kinetic energy dissipation rate, ω. The incompressible transport equations are disclosed in Eq. (14) to Eq. (16):

$$\frac{Dk}{Dt} = P_k + R_{BP} + R_{NAT} - \omega k - D_T + \frac{\partial}{\partial x_j}\left[\left(\nu + \frac{\alpha_t}{\sigma_k}\right)\frac{\partial k}{\partial x_j}\right] \tag{14}$$

$$\frac{Dkl}{Dt} = P_{kl} + R_{BP} - R_{NAT} - D_L + \frac{\partial}{\partial x_j}\left[\nu\frac{\partial kl}{\partial x_j}\right] \tag{15}$$

$$\frac{D\omega}{D}t = C_{\omega_1}\frac{\omega}{k}P_k + \left(\frac{C_{\omega R}}{f}w - 1\right)\frac{\omega}{k}(R_{BP} + R_{NAT}) - C_{\omega_2}\omega^2 + C_{\omega_3} f_\omega \alpha_T f_W^2 \frac{\sqrt{k}}{y^3} + \frac{\partial}{\partial x_j}\left[\left(\nu + \frac{\alpha_t}{\sigma_\omega}\right)\frac{\partial \omega}{\partial x_j}\right] \tag{16}$$

The production terms in Eq. (14) and Eq. (15) are based on velocity strain rate and are presented in Eq. (17) and Eq. (18)

$$P_k = \nu_{T,s} S^2 \tag{17}$$

$$P_{kl} = \nu_{T,l} S^2 \tag{18}$$

One of the most interesting features of this transition model is the turbulence scale division. Introduced in the work of Walters and Leylek [14], this was also applied in the 2008 $k-kl-\omega$ version [22]. This concept has been shown to be present in fully turbulent boundary layers by Moss and Oldfield [23] and Thole and Bogard [24]. As such, turbulence is divided in large and small scales. The large scale is related to the laminar fluctuation kinetic energy production through the "splat mechanism", as suggested by Volino [25] and mentioned by Bradshaw [26]. The small scale is related to regular turbulence. Far from wall surfaces the small scale turbulent kinetic energy is equal to the free-stream turbulent kinetic energy. The definition of the limiting length scale is obtained from Eq. (19), where λ_T is the turbulent small length scale defined in Eq. (20):

$$\lambda_{eff} = \min(C_{\lambda y}, \lambda_T) \tag{19}$$

$$\lambda_T = \frac{\sqrt{k}}{\omega} \tag{20}$$

The small scale turbulent kinematic viscosity is calculated as presented in Eq. (21). This makes use of a collection of damping functions that attempt to simulate various mechanisms, such as the shear-sheltering effect (see Eq. (22)), the turbulence intermittency (see Eq. (23)) and the kinematic and viscous wall effect as presented in Eq. (24) and Eq. (25). The last damping function is based on effective turbulent Reynolds number (see Eq. (26)). Furthermore, in order to satisfy realizability, C_μ is calculated according to Eq. (27). In the work of Walters et al. [14,22], C_μ is a simplified version of its original form according to the work of Shih and Zhu [27] and Shih et al. [28].

$$\nu_{T,s} = f_v f_{INT} C_\mu \sqrt{k_{T,s}}\lambda_{eff} \tag{21}$$

$$f_{SS} = e^{[-(\frac{C_{SS}\nu\Omega}{k})^2]} \tag{22}$$

$$f_{INT} = \min\left(\frac{k_L}{C_{INT}k_{TOT}}, 1\right) \tag{23}$$

$$f_W = \frac{\lambda_{eff}}{\lambda_T} \tag{24}$$

$$f_v = 1.0 - e^{-\frac{\sqrt{Re_T}}{A_v}} \tag{25}$$

$$Re_T = \frac{f_W^2 k}{\nu\omega} \tag{26}$$

$$C_\mu = \frac{1}{A_0 + A_s(\frac{S}{\omega})} \tag{27}$$

The remaining $k-kl-\omega$ transition model description can be found in the work of Walters and Cokljat [22]. The described transition model was implemented in the open-source software OpenFoam. After a systematic analysis and testing of the transition model some modifications were proposed. Application of such modifications yielded improved results. One of the applied changes to the model was made to the turbulence intermittency damping function f_{INT} (see Eq. (23)). This modification avoids the fact that the original model predicts zero turbulent viscosity in the free-stream. This is so since k_L exists only near wall surfaces. Therefore the proposed term is then calculated as presented in Eq. (28).

$$f_{INT}^{new} = \min\left(\frac{k}{C_{INT}k_{TOT}}, 1\right) \tag{28}$$

Another relevant change in relation to the original model is the definition of turbulence Reynolds number, Re_T presented in Eq. (26). The classical literature definition of turbulence Reynolds number as used by several turbulence models such the ones presented at Refs. [29–31] was applied also in the present modified transition model. This will result in an improved asymptotic skin-friction coefficient behavior along the fully turbulent region of the flow. The altered term is presented in Eq. (29):

$$Re_T^{new} = \frac{k}{\nu\omega} \tag{29}$$

The original model's turbulence specific dissipation rate destruction term is $-C_{\omega 2}\omega^2$. It was observed that the latter had an excessive effect near the wall. Also, in the work of Craft et al. [32] the presented turbulence model has a set of equations resembling the presented turbulent kinetic energy, k, and the specific turbulent kinetic energy dissipation rate, ω, of the $k-kl-\omega$ transition model. In the just presented work, instead of ω, the transported quantity is the turbulent kinetic energy dissipation rate, $\tilde{\epsilon}$. The function of interest is $C_{\epsilon 2}$. This is multiplied by the term responsible for the destruction of the turbulent kinetic energy dissipation rate. Near the wall, its influence is reduced. The proposed hypothesis is then the imposition of a damping function, f_ω (see Eq. (24)) multiplied to the $-C_{\omega 2}\omega^2$ term. The resulting term is given in the third element on the right side of Eq. (30):

$$\frac{D\omega}{Dt} = C_{\omega 1}\frac{\omega}{k}P_k + \left(\frac{C_{\omega R}}{f_W} - 1\right)\frac{\omega}{k}(R_{BP} + R_{NAT}) - C_{\omega 2}\omega^2 f_W + C_{\omega 3} f_\omega \alpha_T f_W^2 \frac{\sqrt{k}}{y^3} + \frac{\partial}{\partial x_j}\left[\left(\nu + \frac{\alpha_t}{\sigma_\omega}\right)\frac{\partial \omega}{\partial x_j}\right] \tag{30}$$

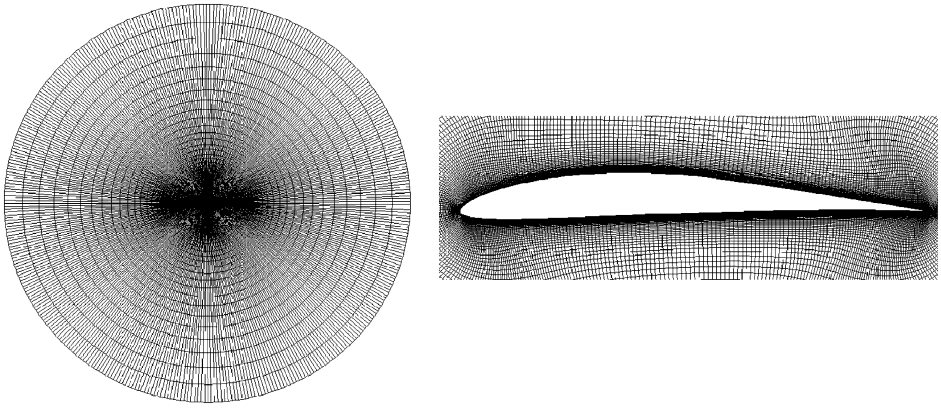

Fig. 1. (a) General view of the used mesh for the CFD simulations. (b) Detail of the mesh around the airfoil.

A more detailed description of the modified $k-kl-\omega$ turbulence transition model version is available in the work of Vizinho et al. [12].

2.3. XFOIL code

The XFOIL [13] code combines a potential flow panel method and an integral boundary layer formulation for the analysis of the flow around airfoils. The code was developed to rapidly predict the airfoil performance at low Reynolds numbers and its convergence is achieved through the iteration between the outer and inner flow solutions on the boundary layer displacement thickness. Thus, the XFOIL code calculates the viscous pressure distribution and captures the influence of limited trailing edge separation and laminar separation bubbles. The XFOIL uses an approximate e^N envelope method to calculate transition. With this method the code tracks only the most amplified frequency at a given point on the airfoil downstream from the point of instability to obtain the amplitude of that disturbance. Transition is assumed when this integrated amplitude reaches an empirically determined value. The appropriate N to use into XFOIL calculations, can be calculated by Eq. (31) as presented by van Ingen [33].

$$N = -8.43 - 2.4\ln(T_u) \tag{31}$$

where T_u represents the absolute turbulence intensity. In the present work N was set to the default value of 9, which corresponds to a smooth wing surface in a low turbulence intensity freestream.

3. Numerical procedure

3.1. Mesh generation

In order to simulate the airfoils and compare the different Computational Fluid Dynamics (CFD) models, a completely structured O-type mesh was used. The mesh had the outer boundaries placed 30 chords away from the airfoil. The airfoil was defined with 250 points around its contour and special attention was given to the boundary layer regions in order to ensure that the first point of the mesh corresponds to a $y^+ < 1$. The used mesh is shown in Fig. 1.

3.2. Boundary conditions

To simulate the airfoils at the desired chord-based Reynolds number, corresponding to those of the available experimental results given by the literature ($Re = 2.0 \times 10^5$), a density based solver was applied. The far boundary was represented by a pressure farfield using the Mach number input to prescribe the flow speed. The desired angle of attack was obtained using the appropriate flow direction vector components. The airfoil top and bottom surfaces were defined as wall boundary conditions and the fluid inside the domain was defined as air with $\rho = 1.225$ kg/m^3 and $\mu = 1.79 \times 10^{-5}$ Pa s. These procedures give the advantage to simulate all angles of attack using only a single mesh [34]. To correctly compute the lift and drag coefficients, the decomposition of the flow direction vector was used as presented in Eq. (32) and Eq. (33)

$$L = L'\cos(\alpha) - D'\sin(\alpha) \tag{32}$$

$$D = L'\sin(\alpha) + D'\cos(\alpha) \tag{33}$$

where L and D are lift and drag, respectively, and L' and D' represent the components of the aerodynamic force based on the mesh system of coordinates of Ansys Fluent®.

3.3. CFD simulation procedure

Both Computational Fluid Dynamics simulations were performed using a steady state solver. The pressure based solver, SIMPLE, was used together with a Green-Gauss cell based discretization scheme. On Ansys Fluent®, a second order upwind (SOU) scheme was used for the momentum and turbulence equations discretization. Regarding the OpenFoam simulations, the second order linear-upwind stabilized transport (LUST) discretization scheme was chosen. The Laplacian terms and the pressure equations were discretized using a linear discretization. The convergence of the numerical solution is controlled considering suitable under relaxation factors for the turbulent variables. Convergence is also guaranteed by monitoring the relative numerical error of the solution, as it drops below 1.0×10^{-8}. In order to compare the results of the numerical simulations with the obtained results from the JBLADE software, the airfoils were simulated for a given Reynolds number, over a range of angles of attack.

3.4. XFOIL simulation procedure

The influence of the number of points used to define the airfoil inside XFOIL was analyzed. Fig. 2 presents the different polars obtained using different number of points in XFOIL. It was concluded that for more than 150 points, XFOIL does not show a significant difference in the airfoil polars. However, as the XFOIL is requiring less than a minute of elapse time per polar on an average desktop computer, each airfoil was defined with 250 points.

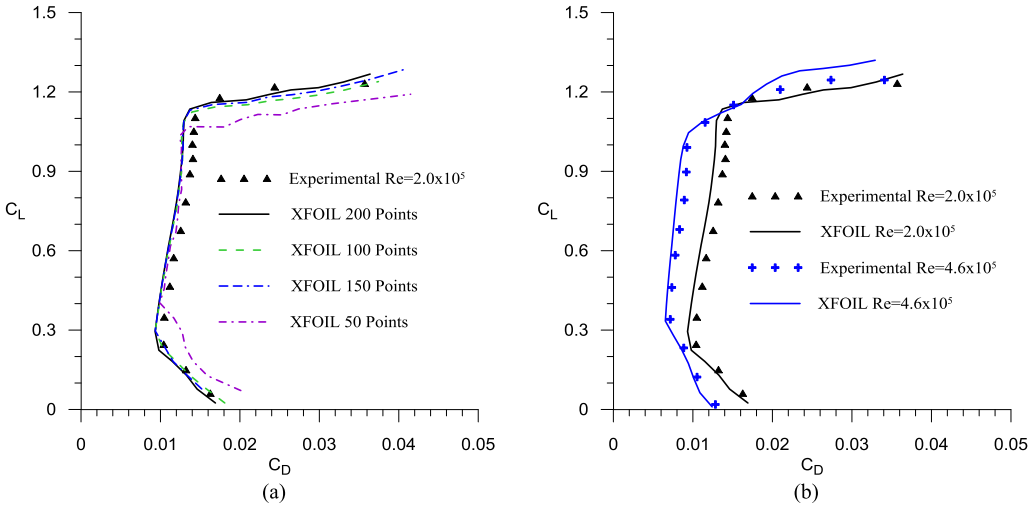

Fig. 2. (a) Validation of polar calculation using different number of points to define an airfoil in XFOIL. (b) Comparison between XFOIL and experimental studies [35] for E387 airfoil at different Reynolds numbers.

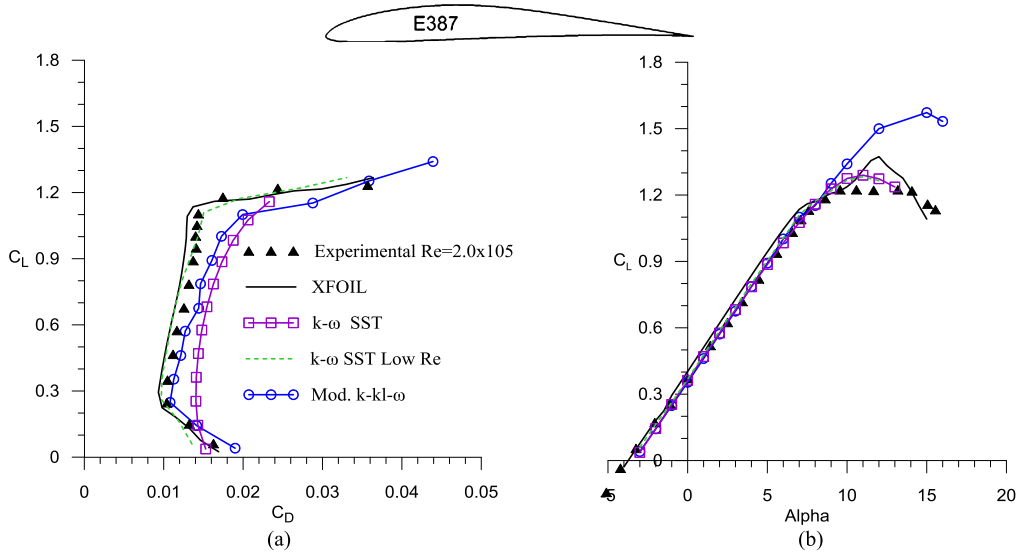

Fig. 3. Aerodynamic characteristics of the E387 airfoil measured at Penn State wind tunnel [37] compared with the numerical simulation results. (a) C_L *vs* C_D. (b) C_L *vs* α.

4. Results and discussion

4.1. E387 airfoil

The *E*387 airfoil was designed during 1960s by Richard Eppler. Since the airfoil was specifically designed to use on model sailplanes, it had represented a significant improvement over other airfoils available at that time. The airfoil performance predicted for $Re = 2.0 \times 10^5$ by XFOIL, $k-kl-\omega$ transition model and $k-\omega$ *SST* turbulence model (with and without low Reynolds corrections) are compared to the University of Illinois Urbana–Campaign (UIUC) [35] wind-tunnel measurements in Fig. 3(a) and (b).

The results presented at Fig. 3(a) show that all the predictions are in good agreement with the experiments. The XFOIL and $k-SST$ turbulence model with the low Reynolds corrections ($k-\omega$ *SST Low Re*) are capable to accurately predict the corners of the low drag region, although they are predicting a slightly higher maximum lift coefficient. Regarding the $k-\omega$ *SST* without low Reynolds corrections, since it is unable to predict transition, it does not replicate the sharp corners, although the maximum lift coefficient is well computed.

The refurbished version of $k-kl-\omega$ transition model presents better agreement with the experimental data than *SST* $k-\omega$ turbulence model without low Reynolds corrections. For the lower corner of the low drag bucket this model can correctly predict the values of both lift and drag coefficients. In the direction of the top corner of the low drag region as the lift coefficient increases $k-kl-\omega$ transition model predicts a slightly higher drag coefficient for a given lift coefficient, making the curve appear to the right when compared with the measurements.

Fig. 4(a) and (b) shows the pressure distribution for an angle of attack of 0 and 4 degrees, respectively. The results obtained from the described numerical methods are compared with the measurements provided in Ref. [36].

At an angle of attack of 0°, XFOIL and $k-\omega$ *Low Re* turbulence model are in a perfect agreement with experiments, while the modified $k-kl-\omega$ transition model slightly under predicts the pressure coefficient in the upper surface of the airfoil. At the angle of attack of 4°, the behavior of different used methods remain the same, with a slightly under prediction in the $k-kl-\omega$ transition model until $x/c = 0.6$.

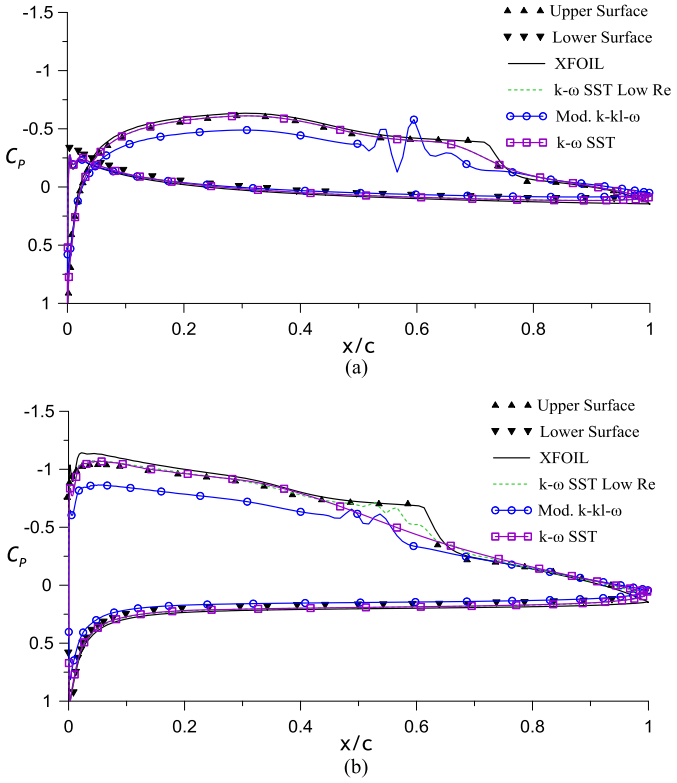

Fig. 4. Comparison of E387 airfoil pressure distributions for $Re = 2.0 \times 10^5$ [36]. (a) $\alpha = 0°$. (b) $\alpha = 4°$.

In Fig. 5(a) the transition position versus lift coefficient is plotted with the airfoil's drag polar in order to observe the parallelism between the position of the transition and the laminar bucket limits. It is clear that the less steep part of the transition curves correspond to the limits of the laminar bucket of the drag polar as shown in Fig. 5.

In particular, one can note the lift coefficient of the transition ramps as the corners of the low drag bucket of the airfoil. The lower surface transition ramp at lift coefficient of about 0.3 as the lower corner and the upper surface transition ramp at lift coefficient of about 1.15 as the upper corner of the low drag bucket. The turbulence model *SST* $k-\omega$ with low Reynolds corrections and XFOIL give a close prediction but the latter estimates a larger laminar flow extent at lower lift coefficients. The modified $k-kl-\omega$ transition model shows the same trend but only matches closely the other models around a lift coefficient of 1.18, overestimating the laminar flow extent at higher lift coefficients. The relation between transition position and laminar bucket of the drag polar demonstrates the importance of the transition location prediction during the development of a new airfoil.

4.2. S1223 airfoil

The S1223 airfoil was designed by M. Selig [35] to achieve a $Cl_{\max}$ greater than 2 at $Re = 2.0 \times 10^5$. The S1223 airfoil has 11.93% thickness and camber of 8.67%. The UIUC [35] experimental data give a maximum lift coefficient of approximately 2.2 with moderate stall characteristics as shown in Fig. 6(a) and (b).

Fig. 6(a) shows the predictions for the S1223 airfoil drag polar. For the $k-\omega$ *SST* turbulence model with low Reynolds corrections, the agreement with experimental data is good up to an angle of attack of approximately 10°. Contrary to the predictions presented for the E387 airfoil, the $k-kl-\omega$ transition model does not predict the lower corner of the low drag bucket accurately. However, the agreement for higher angles of attack is even better than the XFOIL predictions. For XFOIL, the maximum lift coefficient is well predicted although it occurs in a lower angle of attack, as it is possible to observe in Fig. 6(b). At higher angles of attack XFOIL underestimates, by a significant extent, the drag coefficient value.

Fig. 7(a) shows the pressure distribution at $\alpha = 4°$ and it is possible to observe that, according to the comparison provided in Fig. 4 (a) and (b) the $k-\omega$ *SST Low Re* represents the most accurate approximation to the experiments. While the $k-kl-\omega$ transition model is slightly underestimating the correct pressure distribution, the XFOIL code is overestimating the pressure distribution around the airfoil for this angle of attack. At Fig. 7(b) the pressure distribution for $\alpha = 8°$ shows the same above mentioned behavior of each model.

5. Conclusions

Analyzing the comparisons between the experimental measurements and the predictions obtained using different numerical methods, it is clear that the XFOIL remains an excellent airfoil design and analysis tool. It shows the capability to predict the airfoil performance as good as any of the other used methods. The ease of use of XFOIL compared to the more complex CFD performed in ANSYS Fluent® and OpenFoam encourages its use at low speeds

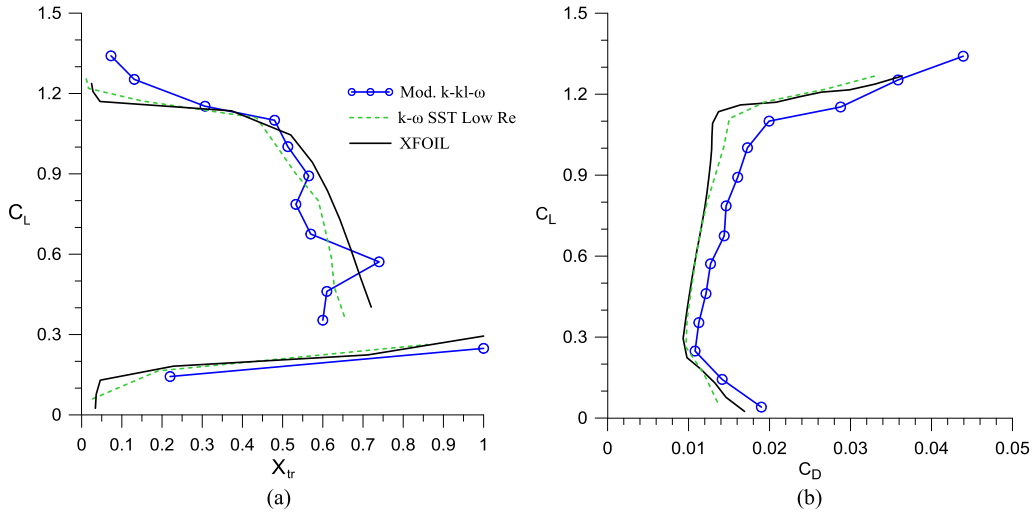

Fig. 5. (a) Transition position of the E387 airfoil. (b) Drag polar of E387 for $Re = 2.0 \times 10^5$.

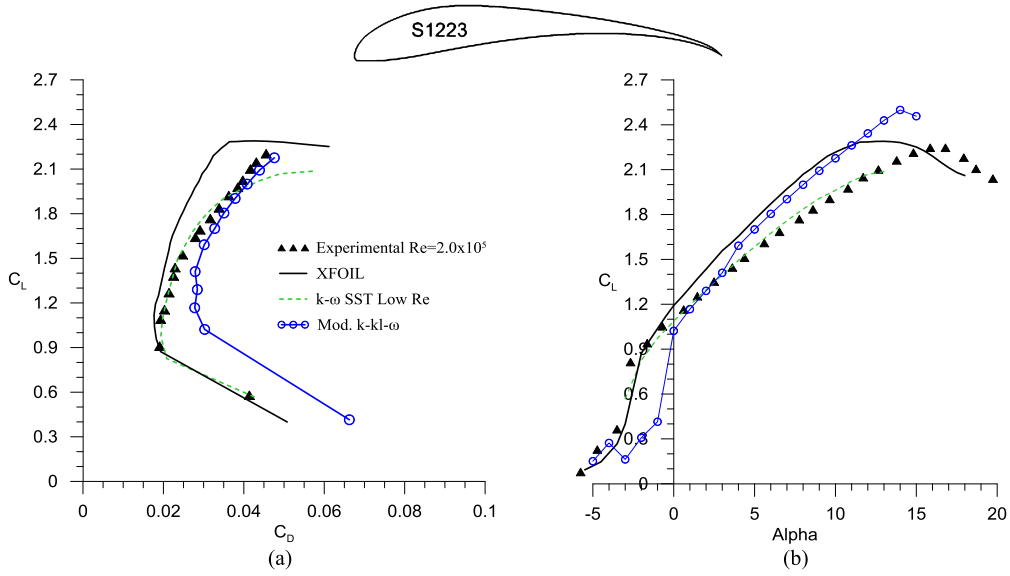

Fig. 6. S1223 airfoil polar for $Re = 2.0 \times 10^5$. UIUC measurements from Ref. [35] (a) C_L *vs* C_D. (b) C_L *vs* α.

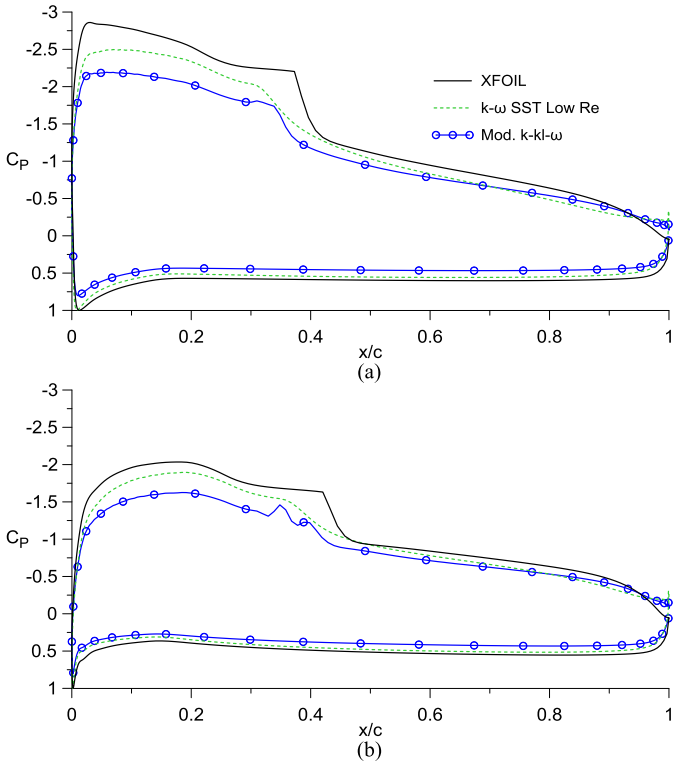

Fig. 7. Comparison of S1223 airfoil pressure distributions for $Re = 2.0 \times 10^5$. (a) $\alpha = 4°$. (b) $\alpha = 8°$.

and for single-element airfoils. XFOIL predictions are comparable to those of other turbulence and transition methods. Although only two cases were considered, the changes made in the $k - kl - \omega$ transition model shows promising results in predicting accurate C_L and C_D values. It was clear that a number of existing methods can predict the aerodynamic characteristics of airfoils with sufficient accuracy for most engineering applications. While XFOIL can provide sufficient accuracy for the conceptual design phase of the propellers, the importance of being able to account for transition with Navier–Stokes solvers is of high importance, not only for steady-state two-dimensional calculations, but also for the three-dimensional and/or unsteady-state cases.

Conflict of interest statement

The authors declare that there is no conflict of interests regarding the publication of this article.

Acknowledgements

The present work was performed as part of Project MAAT (Ref. No. 285602) supported by European Union through the Seventh Framework Programme. Part of the work was also supported by C-MAST – Center for Mechanical and Aerospace Sciences and Technologies, Portuguese Foundation for Science and Technology Research Unit No. 151.

References

[1] R. Ma, B. Zhong, P. Liu, Optimization design study of low-Reynolds-number high-lift airfoils for the high-efficiency propeller of low-dynamic vehicles in stratosphere, Sci. China, Technol. Sci. 53 (2010) 2792–2807, http://dx.doi.org/10.1007/s11431-010-4087-0.
[2] B.E. Prentice, A. Phillips, R.P. Beilock, J. Thomson, The rebirth of airships, J. Transp. Res. Forum 44 (2005) 173–190.
[3] G. Ilieva, J.C. Páscoa, A. Dumas, M. Trancossi, A critical review of propulsion concepts for modern airships, Cent. Eur. J. Eng. 2 (2012) 189–200, http://dx.doi.org/10.2478/s13531-011-0070-1.
[4] A. Dumas, M. Trancossi, M. Madonia, I. Giuliani, Multibody advanced airship for transport, in: SAE Technical Paper 2011-01-2786, 2011.
[5] J. Morgado, M.Â.R. Silvestre, J.C. Páscoa, Parametric study of a high altitude airship according to the multi-body concept for advanced airship transport – MAAT, in: IV Conferência Nacional Em Mecânica Dos Fluidos, Termodinâmica E Energia, Lisbon, 2012.
[6] J. Morgado, M. Abdollahzadeh, M.A.R. Silvestre, J.C. Páscoa, High altitude propeller design and analysis, Aerosp. Sci. Technol. 45 (2015) 398–407, http://dx.doi.org/10.1016/j.ast.2015.06.011.
[7] M. Young, S. Keith, An overview of advanced concepts for near-space systems, in: 45th AIAA Joint Propulsion Conference & Exhibit, American Institute of Aeronautics and Astronautics, Denver, Colorado, 2009.
[8] L.D. Koch, Design and performance calculations of a propeller for very high altitude flight, Case Western Reserve University, 1998.
[9] P.V. Gamboa, M.A.R. Silvestre, Airfoil optimization with transition curve as objective function, in: VI International Conference on Adaptive Modeling and Simulation ADMOS 2013, 2013, pp. 1–12.
[10] F.R. Menter, Two-equation eddy-viscosity turbulence models for engineering applications, AIAA J. 32 (1994) 1598–1605, http://dx.doi.org/10.2514/3.12149.
[11] F.R. Menter, Influence of freestream values on k–omega turbulence model predictions, AIAA J. 30 (1992) 1657–1659, http://dx.doi.org/10.2514/3.11115.
[12] R. Vizinho, J.C. Pascoa, M. Silvestre, High altitude transitional flow computation for a propulsion system nacelle of MAAT airship, SAE Int. J. Aerosp. 6 (2013) 714–720, http://dx.doi.org/10.4271/2013-01-2268.

[13] M. Drela, XFOIL – an analysis and design system for low Reynolds number airfoils, in: T.J. Mueller (Ed.), Low Reynolds Number Aerodynamics, Springer-Verlag, Berlin, 1989, pp. 1–12.
[14] D.K. Walters, J.H. Leylek, A new model for boundary layer transition using a single-point RANS approach, J. Turbomach. 126 (2004) 193, http://dx.doi.org/10.1115/1.1622709.
[15] M.S. Selig, Low Reynolds number airfoil design lecture notes, VKI Lect. Ser. (2003) 24–28.
[16] J. Bardina, P. Huang, T. Coakley, J. Bardina, P. Huang, T. Coakley, Turbulence modeling validation, in: 28th Fluid Dynamics Conference, American Institute of Aeronautics and Astronautics, Reston, Virigina, 1997.
[17] R.E. Mayle, A. Schulz, The path to predicting bypass transition, in: Volume 1: Turbomachinery, ASME, 1996, pp. 405–411.
[18] H. Dryden, Air flow in the boundary layer near a plate, NACA report 562, 1937.
[19] G. Taylor, Some recent developments in the study of turbulence, in: Fifth International Congress for Applied Mechanics, Cambridge, Massachusetts, 1939.
[20] P. Klebanoff, Effects of free-stream turbulence on a laminar boundary layer, Bull. Am. Phys. Soc. 16 (1971) 1323.
[21] J. Kendall, Studies on laminar boundary layer receptivity to freestream turbulence near a leading edge, in: Boundary Layer Stability and Transition to Turbulence, in: Proceedings of the Symposium, ASME and JSME Joint Fluids Engineering Conference, 1991.
[22] D.K. Walters, D. Cokljat, A three-equation eddy-viscosity model for Reynolds-averaged Navier–Stokes simulations of transitional flow, J. Fluids Eng. 130 (2008) 121401, http://dx.doi.org/10.1115/1.2979230.
[23] R. Moss, M. Oldfield, Effect of free-stream turbulence on flat-plate heat flux signals: spectra and eddy transport velocities, J. Turbomach. 118 (1996) 461–467.
[24] K. Thole, D. Bogard, High freestream turbulence effects on turbulent boundary layers, J. Fluids Eng. 118 (1996) 276–284.
[25] R.J. Volino, A new model for free-stream turbulence effects on boundary layers, J. Turbomach. 120 (1998) 613–620.
[26] P. Bradshaw, Turbulence: the chief outstanding difficulty of our subject, Exp. Fluids 16 (1994) 203–216, http://dx.doi.org/10.1007/BF00206540.
[27] T. Shih, J. Zhu, J. Lumley, A new reynolds stress algebraic equation model, NASA TM 106644, Ohio, 1994.
[28] T.-H. Shih, W.W. Liou, A. Shabbir, Z. Yang, J. Zhu, A new $k-\epsilon$ eddy viscosity model for high Reynolds number turbulent flows, Comput. Fluids 24 (1995) 227–238, http://dx.doi.org/10.1016/0045-7930(94)00032-T.
[29] K.C. Chang, W.D. Hsieh, C.S. Chen, A modified low-Reynolds-number turbulence model applicable to recirculating flow in pipe expansion, J. Fluids Eng. 117 (1995) 417–423, http://dx.doi.org/10.1115/1.2817278.
[30] T.J. Craft, B.E. Launder, K. Suga, Prediction of turbulent transitional phenomena with a nonlinear eddy-viscosity model, Int. J. Heat Fluid Flow 18 (1997) 15–28, http://dx.doi.org/10.1016/S0142-727X(96)00145-2.
[31] S. Lardeau, M.A. Leschziner, N. Li, Modelling bypass transition with low-Reynolds-number nonlinear eddy-viscosity closure, Flow Turbul. Combust. 73 (2004) 49–76, http://dx.doi.org/10.1023/B:APPL.0000044367.24861.b7.
[32] T.J. Craft, B.E. Launder, K. Suga, Development and application of a cubic eddy-viscosity model of turbulence, Int. J. Heat Fluid Flow 17 (1996) 108–115.
[33] J. van Ingen, The eN method for transition prediction. Historical review of work at TU delft, in: 38th Fluid Dynamics Conference and Exhibit, American Institute of Aeronautics and Astronautics, Reston, Virigina, 2008.
[34] D. Silva, M. Avelino, M. De-Lemos, Numerical study of the airflow around the airfoil S1223, in: II Congresso Nacional de Engenharia Mecânica, João Pessoa, 2002.
[35] M.S. Selig, J.J. Guglielmo, High-lift low Reynolds number airfoil design, J. Aircr. 34 (1997) 72–79, http://dx.doi.org/10.2514/2.2137.
[36] R. McGee, B. Walker, B. Millard, Experimental results for the eppler 387 airfoil at low Reynolds numbers in the langley low-turbulence pressure tunnel, Hampton, Virginia, 1988.
[37] M.D. Maughmer, J.G. Coder, Comparisons of theoretical methods for predicting airfoil aerodynamic characteristics, Pennsylvania State University, 2010.